Behavioral/Systems/Cognitive

Deterministic Multiplicative Gain Control with Active Dendrites

W. Hamish Mehaffey,[1] Brent Doiron,[2,3] Leonard Maler,[3] and Ray W. Turner[1]

[1]Hotchkiss Brain Institute, University of Calgary, Calgary, Alberta, Canada T2N 4N1, and [2]Department of Physics and [3]Cellular and Molecular Medicine, University of Ottawa, Ottawa, Ontario, Canada K1N 6N5

Multiplicative gain control is a vital component of many theoretical analyses of neural computations, conferring the ability to scale neuronal firing rate in response to synaptic inputs. Many theories of gain control in single cells have used precisely balanced noisy inputs. Such noisy inputs can degrade signal processing. We demonstrate a deterministic method for the control of gain without the use of noise. We show that a depolarizing afterpotential (DAP), arising from active dendritic spike backpropagation, leads to a multiplicative increase in gain. Reduction of DAP amplitude by dendritic inhibition dilutes the multiplicative effect, allowing for divisive scaling of the firing rate. In contrast, somatic inhibition acts in a subtractive manner, allowing spatially distinct inhibitory inputs to perform distinct computations. The simplicity of this mechanism and the ubiquity of its elementary components suggest that many cell types have the potential to display a dendritic division of neuronal output.

Key words: **gain control; sensory processing; electric fish; dendrite; backpropagation; division**

Introduction

Individual neurons integrate synaptic inputs and output action potentials (spikes) to convey information. The ability of neurons to divisively modulate their firing rate, rather than simply summating inhibitory and excitatory synaptic events, represents a significant increase in complexity for single neuron computation. Division or multiplication of firing rate by synaptic input, originally suggested by Reichardt (1961), has since become a key component of many models of neural processing (Salinas and Sejnowski, 2001) and is required in models characterizing the response of cells in the visual cortex (Carandini and Heeger, 1994) and efficient coding in visual and auditory systems (Schwartz and Simoncelli, 2001). Early investigations into biophysical mechanisms for division of firing rate were based on Ohm's law: membrane potential is equal to current divided by membrane conductance (Blomfield, 1974; Koch and Poggio, 1992; Nelson, 1994). Divisive changes in membrane potential resulting from increased conductance were assumed to translate to a division of firing rate. Later theoretical studies showed that shunting inhibition is unable to divisively modulate firing rate (Gabbiani et al., 1994; Holt and Koch, 1997). Instead, changes in subthreshold membrane conductance led to primarily inhibitory effects on spiking, causing a subtractive shift in the onset of firing in the cell.

Since this time, a number of studies have sought to determine a mechanism allowing synaptic regulation of the gain of an individual cell. Dynamic clamp (Chance et al., 2002; Mitchell and Silver, 2003) and modeling of various configurations of synaptic input (Salinas and Sejnowski, 2000; Tiesinga et al., 2000; Doiron et al., 2001b; Longtin et al., 2002; Burkitt et al., 2003; Prescott and De Koninck, 2003) have shown that noise can generate divisive effects. These studies indicate that after balancing of stochastic inputs, frequency–current (FI) curves have a stationary current threshold for initial spiking (rheobase) while the gain (in hertz/nanoampere) decreases. However, studies of noise-induced gain have used the variance in membrane fluctuation to drive spiking in a probabilistic manner. This suggests that as the time window used to calculate average spike rate is increased, the likelihood of successfully encoding transient inputs may be reduced.

We show that proximal dendritic inhibition is capable of regulating a dendrosomatic current flow arising from backpropagating dendritic spikes. This gives rise to a novel form of deterministic regulation of the gain of the spike generating mechanism, distinct from all previous mechanisms that required balanced, noisy synaptic conductance changes near the spike generating mechanism. The biophysical components required for dendritic division of neuronal inputs are simple and widespread and may thus be used in many other systems.

Materials and Methods

Preparation of slices. Weakly electric brown ghost knife fish (*Apteronotus leptorhynchus*) were obtained from local importers and maintained at 26–28°C in fresh water aquaria, in accordance with protocols approved by the University of Calgary Animal Care Committee. All chemicals were obtained from Sigma (St. Louis, MO) unless otherwise noted. In all cases, recordings were obtained from separate pyramidal cell somata or apical

Received June 29, 2005; revised Sept. 9, 2005; accepted Sept. 19, 2005.

This work was supported by the Canadian Institutes of Health Research (CIHR) (L.M., R.W.T.), the Alberta Heritage Foundation for Medical Research (AHFMR) Scientist Award (R.W.T.), the Ontario Graduate Scholarship in Science and Technology (B.D.), the Province of Alberta Graduate Scholarship, and CIHR and AHFMR studentships (W.H.M.). We thank J. E. Lewis, J. Bastian, and M. J. Chacron for comments on this manuscript and J. Benda and J. E. Lewis for helpful discussions. We thank J. Bastian for permitting the use of his published data.

Correspondence should be addressed to W. Hamish Mehaffey, Hotchkiss Brain Institute, University of Calgary, 3330 Hospital Drive Northwest, Calgary, Alberta, Canada T2N 4N1. E-mail: whmehaff@ucalgary.ca.

B. Doiron's present address: Center for Neural Science, New York University, New York, NY 10003.

DOI:10.1523/JNEUROSCI.2682-05.2005

 0270-6474/05/259968-10$15.00/0

dendrites in the *in vitro* slices. Animals were anesthetized in 0.05% phenoxy-ethanol, and tissue slices of 300–400 μm thickness were prepared from the electrosensory lateral line lobe (ELL) as described previously (Turner et al., 1994). Slices were maintained by constant perfusion of artificial CSF (ACSF; 1–2 ml/min) and superfusion of humidified 95% O_2, 5% CO_2 gas. ACSF contained the following (in mM): 124 NaCl, 3 KCl, 25 $NaHCO_3$, 1.0 $CaCl_2$, 1.5 $MgSO_4$, and 25 D-glucose, pH 7.4. HEPES-buffered ACSF for pressure ejection of pharmacological agents contained the same elements, with the following differences (in mM): 148 NaCl and 10 HEPES.

Stimulation and recording procedures. Glass microelectrodes were backfilled with 2 M KAc, pH 7.4 (90–120 MΩ resistance) and in some recordings contained 2% Neurobiotin (Vector Laboratories, Burlingame, CA). Recordings were made from pyramidal cells ($n = 27$) in the two largest ELL segments receiving amplitude-coded electrosensory inputs (centrolateral and centromedial segments). Cells were identified as bursting or nonbursting by their progression from a tonic to a characteristic firing mode after sufficient depolarization (Turner et al., 1994). Divisive effects were seen in both the tonic and bursting regimes, and the data from both regimes were therefore pooled. Somatic recordings were made from the pyramidal cell layer and dendritic recordings at the boundary of the stratum fibrosum and molecular layer (Turner et al., 1994). Recordings were digitized using an NI PCI-6030E DAQ board (National Instruments, Austin, TX). Intracellular stimuli were delivered, and data were recorded in custom software using the MatLab data acquisition toolbox (MathWorks, Natick, MA). Direct current injection of 0.1–0.6 nA was applied when necessary to eliminate spontaneous discharge. Muscimol (200 μM) was focally ejected over the dendritic or somatic axis using electrodes of 1–2 μm tip diameter and 10–15 psi. A visual estimate of the radius of drug application was initially obtained in dendritic regions under transillumination. Previous studies have shown delays of up to 2 min before drugs ejected in the ventral molecular layer (VML) caused effects at the soma (Turner et al., 1994). Pharmacological agents were dissolved in HEPES-buffered ACSF.

Data analysis. FI curves and analyses of spike parameters were generated using custom software in MatLab. Spike threshold was taken based on the first derivative of the voltage waveform, and slopes of FI curves were calculated from the point of initial spiking to the point of saturation in spike frequency. The size of the afterhyperpolarization (AHP) was defined as the difference in voltage between the threshold point and the minimum voltage of the AHP. Data were plotted in Origin (OriginLab, Northhampton, MA) or Igor Pro (Wavemetrics, Lake Oswego, OR). All statistics are paired *t* tests performed for cells before and after pharmacological manipulation unless otherwise stated. All ranges reported are ±SEM.

Modeling. We used a previously published compartmental reconstruction of an ELL pyramidal cell (Doiron et al., 2001a) to test whether it could replicate our experimental results. Simulations using this large model were run in the NEURON simulation environment (Hines and Carnevale, 1997). To examine the effects of the active dendrite on gain in the most generalizable manner, the burst dynamics specific to these cells were removed. The initial FI curve was refit to allow for a greater multiplicative effect of the depolarizing afterpotential (DAP) in accordance with our dendritic tetrodotoxin (TTX) results. A full summary of all changes is presented in supplemental Table 1 (available at www.jneurosci.org as supplemental material). Note that the Kv3 current has been functionally removed. This current was originally based on kinetics of Kv3.3 channels measured in an expression system (Doiron et al., 2001a). We found that the small active repolarization in the dendrites invoked with these parameters prevented the leak conductance from appropriately replicating our experimental results. Because Kv3 channel kinetics and voltage dependence differ between expression systems and those *in situ* (Baranauskas et al., 2003), this current was functionally removed by setting the parameter to a sufficiently small level to be ineffective.

Because of the variability in initial slopes of FI curves among the cells studied, the firing characteristics of the model cell were modulated to simulate the cell shown in Figure 1 as a representative example. For simulations of synaptic bombardment, 250 excitatory synapses were placed on the basilar bush, the primary site of afferent input to these cells (Maler et al., 1981). All synapses were described by α functions and driven by independent Poisson processes as described previously (Doiron et al., 2001b). Excitatory synapses had a unitary conductance of 300 pS, a time constant (t) of 1.5 ms, and a reversal potential (E_{rev}) of 0 mV (Berman and Maler, 1999). One hundred inhibitory synapses (unitary conductance = 25 pS; $t = 7$ ms; $E_{rev} = -70$ mV) were placed along the apical dendrite in a graded manner, such that <5% of the synapses contacted the 25 μm most proximal to the soma [supplemental Table 2 (available at www.jneurosci.org as supplemental material) gives the gradient used for these simulations]. These synapses are intended to represent the activity of neurons of the VML cells and are in accordance with the pattern of synaptic contact made by these cells (Maler et al., 1981). The same graded distribution of conductances was used in distributing the tonic leak conductances ($E_{rev} = -70$ mV), because the VML cell is the primary GABAergic synapse onto the proximal apical dendrite. For simulation of G2 cell inhibition of pyramidal somata, we used a larger number of synaptic inputs (200–400) stimulated at 100 Hz. The larger number of synapses was required for any noticeable effect to be observed during somatic inhibition and represents the greater GABAergic innervation of the soma (Maler and Mugnaini, 1994).

We use the simple leaky-integrate-and-fire (LIF) model (Lapique, 1907; Koch, 1999) to further study the mechanics of dendritic-dependent divisive gain control. LIF model neurons have a subthreshold membrane potential V_m that evolves according to the following:

$$C\frac{dV_m}{dt} = g(E_r - V_m) + I. \quad (1)$$

g is a passive membrane leak conductance for nonspecific leak channels with a reversal potential E_r, C is the membrane capacitance, and I is the static input current. Equation 1 is supplemented with a firing rule: when $V_m(t) = V_t$, a voltage spike is assumed to have occurred at time t. After the spike, the membrane is reset to a potential $V_r < V_t$. The firing rate f of the model neuron is then simply the inverse of the time T that it takes V_m to raise from V_r to V_t. Explicitly solving Equation 1, T is determined to be:

$$T = \frac{C}{g}\ln\left[\frac{g(V_r - E_r) - I}{g(V_t - E_r) - I}\right]. \quad (2)$$

The model parameters that best mimicked ELL pyramidal cell firing rates were $C = 150$ pF, $E_r = -70$ mV, and $V_t = -55$ mV. V_r varied between -70 and -85 mV, whereas g varied between 5 and 11 nS. With these parameters, the membrane time constant was between 13.6 and 30 ms, which is within the range reported for *in vitro* ELL pyramidal cells (Turner et al., 1994; Berman and Maler, 1999). The qualitative model results presented were not sensitive to these parameters.

Results

Divisive gain control is mediated by dendritic but not somatic inhibition

First-order electrosensory processing in *A. leptorhynchus* is accomplished by pyramidal cells of the ELL. Appropriate input can modulate the firing rate of the pyramidal cell from 0 to 200 Hz (Bastian, 1986). The ELL contains many interneurons that can modify pyramidal cell output (Maler, 1979; Maler and Mugnaini, 1994), and two GABAergic interneurons are especially notable. The G_2 interneuron receives direct electroreceptor input and projects to the pyramidal cell soma. In contrast, inhibitory interneurons of the VML (VML cells) receive descending feedback and project to the region of the apical dendrite that actively propagates sodium spikes (Fig. 1*A*). These inputs are distributed along the proximal dendritic axis, showing a gradient of synaptic density, which peaks ~100 μm from the soma and decays with <5% of contacts in regions near the soma (Maler et al., 1981; Maler and Mugnaini, 1994). In both cases, the inhibition is mediated by the $GABA_a$ receptor subtype (Berman and Maler, 1999). To evaluate the role of these interneurons in the regulation

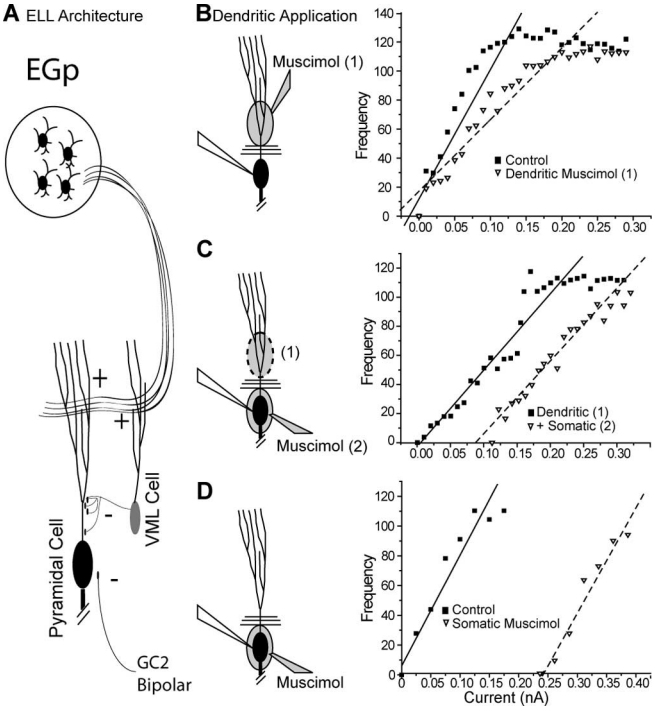

Figure 1. Dendritic inhibitory conductances modulate gain divisively, whereas somatic inhibitory conductances are subtractive. ***A***, Simplified architecture of ELL indirect feedback pathway. Parallel fiber feedback of the eminentia granularis pars posteriori (EGp) cerebellar granule cells drive both the pyramidal cell (black) and the VML cell (gray). The VML cell gives rise to inhibitory synapses contacting the apical dendrites of the pyramidal cell. Inhibitory inputs to the pyramidal cell soma come from many cells including GABAergic granule cells (GC2) and bipolar cells of the nucleus praeminentalis dorsalis (Berman and Maler, 1999). ***B***, Focal application of the $GABA_a$ agonist muscimol (200 μM) to the apical dendrites (▼, dashed line) causes a divisive shift in the FI relationship relative to control (■, solid line) without significantly affecting the rheobase to spiking. ***C***, Application of somatic muscimol subsequent to dendritic ejection (▼, dashed line) fails to further divide the FI curve obtained after dendritic muscimol (■, solid line), having instead a subtractive effect. ***D***, Application of muscimol to the soma alone, in a separate recording, does not shift the slope of the FI curve (▼, dashed line) but shifts the spike rheobase relative to control conditions (■, solid line). Lines in ***B*** and ***C*** are linear fits to the FI plot between rheobase and peak firing frequency. All FI plots have been normalized such that control rheobase is zero.

of sensory processing, we mimicked their activation by focal application of a selective $GABA_a$ agonist, muscimol. Muscimol (200 μM) was applied to either the soma ($n = 9$) or the proximal dendritic region ($n = 14$) of the pyramidal cell while recording from their somata. Because of the architecture of the ELL, we are able to use fiber bundles that bound the pyramidal cell layer as barriers to the diffusion of pharmacological agents and can therefore separate dendritic and somatic effects of applied modulators on cell output (Turner et al., 1994).

We used a series of 500 ms DC current steps to derive FI plots, and the frequency of firing was averaged over the course of the current pulse regardless of discharge pattern (both tonic and bursting modes of discharge were observed, and our results were the same for either pattern). Pharmacological activation of dendritic $GABA_a$ receptors led to a divisive effect on the FI relationship, with minimal effects on the rheobase to commence firing (Fig. 1*B*). Linear fits from the rheobase to the saturation point of the FI curve revealed a significant mean decrease in the slope of 37% (±6.3%; $p < 0.0001$). This slope represents the gain of the firing system in hertz/nanoampere. The rheobase for initial spiking did not change significantly, with a mean value of 0.08 nA (±0.07 nA; $p > 0.15$). The majority ($n = 9$) of these cells showed no or minor subtractive effects (<0.03 nA), whereas one showed very large subtractive effects (0.8 nA), possibly because of muscimol leaking to the somatic region over the course of the experiments (see below). To ensure divisive effects were not a result of the diffusion of pharmacological agents during the recording of individual FI curves, repeated recordings were made after the dendritic muscimol ejection. During drug diffusion, the divisive effects described were reproducible between multiple FI recordings. This indicated that the changes within a single FI curve were not caused by a progressive diffusion of the drug over the course of recording. Rather, it was a result of the continuous activation of $GABA_a$-mediated conductances in the dendritic region over the entire course of the recording.

In contrast, somatic application of muscimol ($n = 3$) had subtractive effects on FI curves (Fig. 1*C*). Somatic application of muscimol immediately after dendritic application ($n = 6$) yielded identical results, with no additional reduction in gain (Fig. 1*D*). Because no differences were noted between the two conditions, the data sets were merged. These experiments showed that somatic muscimol application did not lead to a significant reduction in slope of the FI relationship (5.4 ± 6.5%; $p > 0.45$) but did result in a significant shift in rheobase (0.59 ± 0.16 nA; $p < 0.01$). In an additional two cells, the resulting shift in rheobase was sufficient to prevent firing in response to >1 nA of current injection above the previous rheobase. These cells were not included in the analyses of slope or rheobase, because no spiking was observed.

These differential effects of muscimol would suggest distinct computational properties of dendritic versus somatic inhibition in our cells: dendritic inhibition has a divisive effect, whereas somatic inhibition has subtractive effects, in confirmation of the study by Holt and Koch (1997).

The DAP has an inherently multiplicative effect

In the ELL pyramidal cell, dendritic sodium channels underlie an active backpropagation of the somatic spike through the initial portion of the apical tree (Turner et al., 1994; Lemon and Turner, 2000). These active dendritic conductances result in current flow back to the soma and can create a depolarizing afterpotential (Fig. 2*A*,*B*). Because DAPs arise from active regions of the dendrite that the VML cell selectively inhibits, we examined the contribution of this dendrosomatic current flow to the gain of the firing rate. We blocked the active dendritic conductances by focal application of TTX to the proximal dendritic region ($n = 6$). We monitored these recordings to ensure that TTX was restricted to the dendrites and had not leaked to the soma. No significant decrease in the peak amplitude or rate of rise of the somatic spike was observed (Fig. 2*F*,*G*). Dendritic application of TTX revealed a large somatic AHP, which had been masked previously by the active dendritic conductances (Fig. 2*C*,*F*), whereas the FI curve showed a marked reduction in gain (Fig. 2*H*). This suggests that a significant dendrosomatic current flow exists even when a prominent DAP cannot be observed in the voltage trace.

We further replicated these effects in a large multicompartmental model of an ELL pyramidal neuron (see Materials and Methods), where passive dendrites produced a shallow FI curve. The addition of dendritic Na^+ conductances was sufficient to reproduce an appropriate dendritic spike waveform (Fig. 2*D*), which masked a large portion of the somatic AHP (Fig. 2*E*) and raised the slope of the FI relationship (Fig. 2*I*). These results show that the DAP, a common product of active dendrites, has an inherently multiplicative effect on the FI relationship. Intuitively, this can be understood because the DAP and somatic spike firing

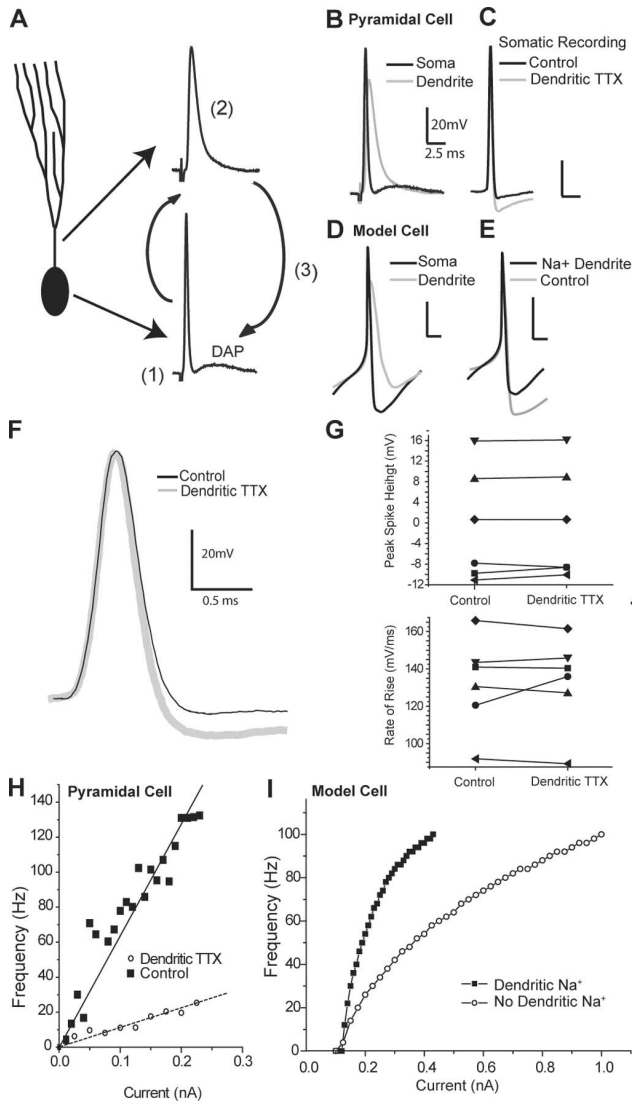

Figure 2. Depolarizing afterpotentials multiplicatively affect the gain of the FI response. ***A***, Schematic diagram of DAP generation by active dendrites: a somatic spike (1) backpropagates into an active dendrite (2), creating a voltage difference between the compartments that leads to dendrosomatic current flow, producing a DAP (3). ***B***, Superimposition of a somatic (black) and a dendritic (gray) spike from separate recordings to show the relationship between the dendritic spike and the DAP. ***C***, Blockade of dendritic sodium channels by application of TTX to the dendrites during somatic recordings removes the DAP and unmasks a large AHP (gray trace) relative to control conditions (black trace) without affecting the height or the shape of the somatic spike. ***D***, Somatic and dendritic spikes in a compartmental model replicate the essential features of spiking seen in the pyramidal cell. ***E***, Masking of the fast AHP by dendrosomatic current flow resulting from backpropagating dendritic spikes in the compartmental model. A large AHP is visible in the case without dendritic sodium (gray) and is partially occluded when active dendritic conductances are included (black). ***F***, Expanded view of ***C*** showing no change in rate of rise of somatic spike height after dendritic TTX ejection. ***G***, Peak amplitude and rate of rise of the somatic spike in six separate experiments are unaffected by dendritic TTX ejection, indicating a specific dendritic effect of TTX. ***H***, Modulation of the FI relationship by active dendritic conductances. Blockade of active dendrite conductances by dendritic application of TTX (○) leads to a much shallower gain in response to step current injections when compared with control condition (■). ***I***, Model results: compared with a passive dendritic model (○), the insertion of conductances generating active dendritic backpropagation leads to a dramatically steeper FI relationship (■).

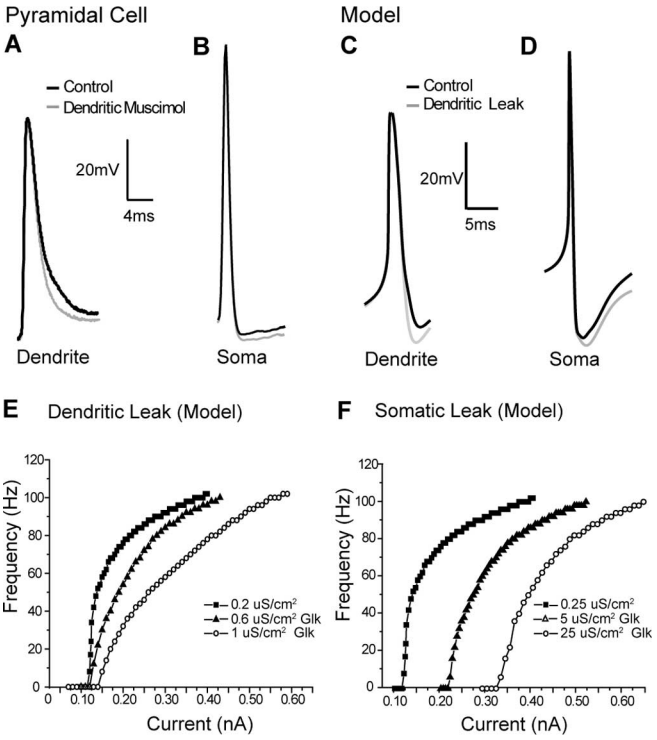

Figure 3. A reduction of the DAP and corresponding increase in AHP divide the FI relationship. ***A***, Application of muscimol to the apical dendrites, whereas recording from dendrites (gray trace) reveals a reduction in the width at the base of the dendritic spike. ***B***, This reduction in dendritic spike width by muscimol is correlated with a larger AHP (gray) relative to control conditions (black) in separate somatic recordings. ***C***, In the compartmental model, the dendritic recording has a faster decay time at its base under "experimental" conditions (increased dendritic G_{lk}, gray) compared with control conditions (normal, black). ***D***, An increase in dendritic leak (0.6 mS/cm ^{2}) leads to a larger AHP at the soma (gray) relative to the control model (black). ***E***, Dendritic leak is sufficient in the model to replicate the gain changes seen experimentally after $GABA_a$ activation. Increasing levels of dendritic leak (3 times, ▲; 5 times, ○) cause divisive effects in the FI relationship compared with control (■). ***F***, In contrast, increasing the somatic leak by 10 times (▲) or 20 times (○) causes purely subtractive shifts without noticeably affecting gain relative to control conditions (■).

are coupled. Specifically, the amount of dendrosomatic current flow scales with firing rate, and the firing rate scales with the amount of dendrosomatic current. The fact that the DAP requires initiation of at least one spike forces rheobase to be invariant with respect to current. This inherent change in firing frequency should occur under any regime in which a backpropagating dendritic spike follows a somatic spike, regardless of their exact shapes. The results obtained from muscimol application (Fig. 1) suggest that this dendritic-dependent multiplicative effect can be diluted by dendritic inhibitory conductances.

The contribution of the DAP can be regulated by dendritic leak conductances

In our system, and in many others, the DAP depends on active dendritic conductances (Turner et al., 1994; Larkum et al., 1996; Magee and Carruth, 1999), and dendritic spikes generally show weak AHPs (Reyes, 2001). Instead, dendrites have a slower process of repolarization. Because we suspected that regulation of active dendritic conductances was involved in modulation of gain, recordings were made from the proximal dendrites of pyramidal cells during focal dendritic application of muscimol (n = 5). Muscimol ejection selectively changed the repolarization phase of dendritic spikes, allowing for a faster decay at the end of the spike (Fig. 3*A*, muscimol trace). These changes in the dendritic spike were seen in separate somatic recordings as a small reduction in the DAP, manifesting itself as a larger AHP after repolarization (Fig. 3*B*). Analysis of the AHPs recorded somatically after dendritic muscimol ejection revealed that under con-

trol conditions, the mean AHP size was 4.85 mV (±0.95 mV), whereas after tonic activation of dendritic $GABA_a$ synapses, the mean AHP size increased to 7.3 mV (±1.67 mV), representing a 35% increase in the size of the AHP (±4.6%; $p < 0.0001$).

Ejections of muscimol to the cell body layer did not create a significant change in AHP size. Under control conditions, the mean AHP size for this population was 6.3 mV, whereas after ejection of somatic muscimol, the mean AHP was 6.65 mV, giving a mean increase of 4.7% ($p > 0.74$). As described above, somatic muscimol ejection did not produce divisive effects but did cause a subtractive change in rheobase for the FI curve. This indicates that dendritic, but not somatic, muscimol application affects the width of the dendritic spike and, subsequently, the size of the somatic AHP. Reductions in dendritic spike width are tied to an increase in the size of the somatic AHP through a reduction in the DAP, which would normally partially mask the fast AHP. Therefore, regulation of the AHP by inhibition is a property exclusive to the apical dendrites of the cell.

Replication of the muscimol experiments in a compartmental model led to similar results; increasing the dendritic leak led to a reduction in spike width during the final decay of the dendritic spike and a slightly lower interspike voltage (Fig. 3*C*). This dendritic change manifested itself as a change in the depth of the somatic AHP (Fig. 3*D*). The modest change in dendritic spike properties and somatic AHP induced by dendritic leak were sufficient to reproduce the changes in gain associated with the modulation of dendritic conductances by muscimol, enabling a fast regulation of the gain; furthermore, dendritic spike width predicted the gain in the firing model (supplemental Fig. 1, available at www.jneurosci.org as supplemental material). Specifically, by increasing the total density of a chloride leak conductance in the dendrites, we were able to significantly shift the gain of the modeled FI relationship with minimal effects on spike rheobase (compare Figs. 3*G* and 1*B*). In comparison, increases in the density of the somatic leak conductance had no change on the gain of the system but instead acted in a purely subtractive manner (compare Figs. 3*F* and 1*C*), a phenomenon that has been well established for somatic inhibition (Gabbiani et al., 1994; Holt and Koch, 1997). This shows that changes in the somatic AHP, on the same scale seen in our data and induced by the same changes in dendritic leak, are capable of producing a divisive change in gain.

Reduced model of divisive computation

Both the experiments and large-scale compartmental modeling suggest that a dendrite capable of action potential backpropagation is a key requirement for this mechanism of gain control. Dendritic TTX results in a larger somatic AHP, because the DAP and AHP overlap in time following a somatic spike, allowing the DAP to mask a fast AHP without otherwise appearing in the voltage trace. An expanded view of the repolarization phase of a somatic action potential shows that a larger somatic AHP results from dendritic TTX application, whereas a similar effect can also be seen in the large compartmental model of a pyramidal cell (Fig. 4*A*, left and center traces). Here, we used a simple LIF model to show how the DAP influence on the AHP is the crucial feature of this mechanism of gain division and to derive specific rules for the sort of manipulations that can lead to divisive gain control.

To model somatic muscimol application, we increased the leak conductance *g*, similar to the strategy used in the large compartmental model. However, standard LIF models lack any formal concept of a spatially extended dendritic tree, making explicit modeling of dendritic muscimol application difficult. Rather than formally incorporate an excitable dendritic membrane dy-

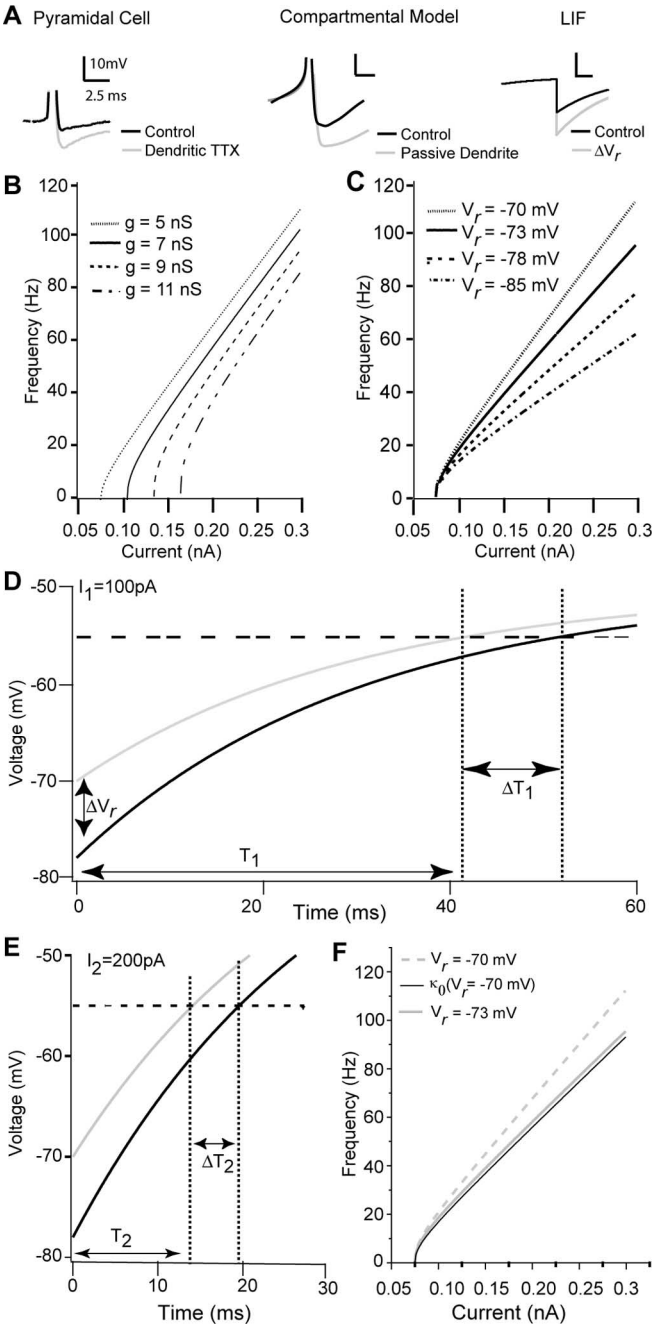

Figure 4. Divisive and subtractive effects can be replicated in an LIF model, allowing for analysis of multiplicative computation. ***A***, Representative changes in somatic AHP resulting from active dendritic conductances in the real cell and compartmental model compared with the reduced LIF model. Gray lines indicate manipulations removing dendritic sodium conductances (left, center) or a change in V_r (right). ***B***, Changes in conductance of the LIF model lead to subtractive shifts in rheobase. As conductance (*g*) increases, rheobase changes, but no change is seen in gain. ***C***, Changes in the reset voltage V_r, simulating regulation of the AHP size by dendritic conductances, lead to divisive changes in gain. As V_r changes, the gain of the LIF cell can be increased or decreased. ***D***, ***E***, For two values of *I*, the change in ISI (*DT*) resulting from a change in AHP (DV_r) scales with the unaltered ISI (*T*). Specifically, for $I_1 = 100$ pA (***D***), the initial ISI (T_1) of the cell is longer than the ISI for $I_2 = 200$ pA (T_2). Importantly, the threshold-crossing delay resulting from the perturbation DV_r when $I = 100$ pA (DT_1) (***D***) is larger than the delay because of the identical perturbation when $I = 200$ pA (DT_2) (***E***). Such scaling of *DT* with *T* shown (***D***, ***E***) is required for DV_r to induce a divisive effect on the FI curve (Eq. 5; see Results). ***F***, The change in gain resulting from the perturbation DV_r is imperfectly described by a single scaling factor k_0 (solid black line), where *k* is independent of the input current *I*.

namic (Larkum et al., 2004), we chose to model and manipulate the effect of dendrosomatic current flow on the somatic AHP. Quite simply, we modeled the somatic effect of dendrosomatic current flow as regulating the depth of the "AHP" [i.e., the membrane potential that the LIF is reset to after a spike (ΔV_r) (Fig. 4*A*, right trace)]. Specifically, a more negative V_r mimics the increase in AHP depth associated with DAP reduction resulting from dendritic muscimol application.

When g is increased (modeling the application of somatic muscimol), we observed a subtractive shift in FI curve gain (Fig. 4*B*). This result has been observed previously in simple IF models and is now a well known effect (Holt and Koch, 1997; Doiron et al., 2001b). Figure 4*C* shows FI curves computed for the LIF model for various values of V_r with g fixed in all cases (modeling the application of dendritic muscimol). When V_r was more negative, a marked decrease in FI slope was observed with no change in the minimal current required for discharge. These results mirror those shown in Figures 1 and 3 for both the experimental and large-scale simulation results. Figure 4*C* shows that simple shifts in action potential reset can account for a divisive gain change. Such a relationship between gain and V_r has been noted previously for LIF models (Troyer and Miller, 1997). However, it has never been interpreted as modeling a variable dendritic feedback to the soma, or any other dynamic process, but has instead been used as a fixed parameter to regulate default gain. With this simple model, we expand on the mechanism to further link the subthreshold dynamics and divisive gain computations.

Specifically, we can define a multiplicative gain change as

$$f'(I) = \kappa(I) f(I), \tag{3}$$

where κ is the factor scaling the original FI curve. A "pure" multiplication will be one that allows $\kappa(I) = \kappa$ so that $f(I)$ is scaled in an input-independent manner during a multiplicative computation. Such a specific definition of multiplicative computations allows for the characterization of simple rules determining the regulation of FI relationships.

It is useful to consider the effects of a gain manipulation in the temporal domain rather than the frequency domain as it appears in Equation 3, because spike firing occurs over time. Using the relationship $T = 1/f$, any manipulation resulting in a multiplicative scaling of the initial FI curve (as defined in Eq. 3) must satisfy the following relationship:

$$\frac{\Delta T(I)}{T(I)} = \frac{1 - \kappa(I)}{\kappa(I)}. \tag{4}$$

Here, $T(I)$ is the original threshold crossing time [e.g., the default interspike interval (ISI)], and $\Delta T(I) = T'(I) - T(I)$ is a decrease (or increase) in that ISI after the gain manipulation. Equation 4 gives a rule for any division of an FI relationship, specifically that in order for a gain manipulation to lead to a divisive computation, it is required that the original period $T(I)$ and the change in period $\Delta T(I)$ scale with each other. Such a rule can be intuitively understood in that to double the frequency of firing at 1 Hz, the period must be advanced by 500 ms, whereas to double the frequency of firing at 10 Hz requires an advance of 50 ms.

Because a shift in V_r induced a slope change in the FI curve in the simple LIF model (Fig. 4*C*), this manipulation is a good candidate to satisfy Equation 4. We show this for two values of input current I_1 (100 pA) and I_2 (200 pA), and for each input we computed $\Delta T(I)$ for models with different voltage resets (ΔV_r) (Fig. 4*D*,*E*). Naturally, as input current increases, the ISI decreases. Interestingly, the effects of ΔV_r grow with T. The resulting effect on the FI curve is a divisive gain change, indicating that to some approximation, our system complies with Equation 4, consistent with the apparent scaling of the FI relationship.

Because our simple LIF system complies with Equation 4 with $\Delta T(I)$ resulting from ΔV_r, we can combine the left side of Equation 4 and the LIF model (Eq. 2) and isolate for $\kappa(I)$ (first equality in Eq. 5). We next considered system parameters that ensure $g(V_r - E_r)/I$, $g(V_r' - E_r)/I$, and $g(V_t - E_r)/I \ll 1$. Specifically, we have these terms ranging from near 0 to 0.5 for the parameters used in Figure 4. We compute the Taylor series expansion of $h(V_r,I)$ and $h(V_r',I)$ using $\ln(1 - x) \approx -x - x^2/2$ for small x (second equality in Eq. 5).

$$\kappa(I) = \frac{h(V_r, I)}{h(V_r', I)} \approx \kappa_0 \left(1 - \frac{g(\Delta V_r)}{1 + g(V_t + V_r' - 2E_r)/I}\right),$$

$$\text{where } h(V, I) = \ln\left(\frac{1 - \frac{g}{I}(V - E_r)}{1 - \frac{g}{I}(V_t - E_r)}\right), \tag{5}$$

and where $k_0 = (V_t - V_r)/(V_t - V_r')$ is the relative change in reset voltage compared with the spike threshold. The expansion shows that although the gain change appears multiplicative (Fig. 4*C*), the neuron model can only exhibit a perfect division of firing rate in the limit in which conductance (g) approaches zero.

Figure 4*F* shows $f(I)$ and $f'(I)$ computed from the LIF model with a 3 mV change in reset voltage. We also plot $f(I)$ multiplied by the zero-order approximation k_0, valid in the limit of zero input conductance. The approximation κ_0 approximately describes the divisive computation for the parameters used in our model.

In our *in vitro* experiments, increased AHP amplitude led to a change in gain, but these two factors were not linearly correlated. This is predicted from our above results, because ELL pyramidal cells have low-input resistances (40–100 MΩ), meaning κ will be a complex function of input current and membrane conductance. Therefore, the range of currents injected and the resting membrane conductance of each cell will have significant effects on attempts to predict κ based on *in vitro* experiments. The above results also show that it is unlikely that a perfect division, in which the firing rate is equally scaled across the entire range of driving currents, will occur. Because cells with large dendritic arborizations have large-input conductances, the scaling of the gain in many cells is likely to be uneven across the FI plot. Although most models involving division of firing rate assume a pure division (Carandini and Heeger, 1994; Schwartz and Simoncelli, 2001), a quasidivisive effect, as seen in our data, will also accomplish this and may even allow for more complex calculations.

Using a simple rule defining the requirements that must be satisfied by any candidate deterministic gain control mechanism (Eq. 4), we examined the LIF system. Because the change in reset voltage in the LIF satisfied this rule and replicated the effects seen in our data and compartmental model, and because prominent DAPs were absent in many of our cells and our compartmental model, we conclude that control of the AHP by the regulation of active dendritic conductances is the key variable defining this gain control mechanism. This AHP scaling mechanism functions through the fundamental integrative properties of the membrane, allowing the time to threshold to vary with the effect of the perturbation resulting from the AHP (Fig. 4).

Divisive gain control by unbalanced synaptic bombardment

The gain control mechanism shown above functions independently of noise. However, noise is an important component of neural systems and is key to the functioning of all previous mechanisms that have successfully controlled gain in a single cell (Doiron et al., 2001b; Chance et al., 2002; Mitchell and Silver, 2003; Prescott and De Koninck, 2003). To examine the interactions between our mechanism and synaptic noise, we simulated stochastic synaptic inputs to examine the more realistic noisy scenario. We distributed 250 excitatory synapses along the basal bush of the pyramidal cell model, consistent with morphological data (L. Maler, unpublished observation) and a previous study of noise-induced gain control in this model (Longtin et al., 2002), giving us a more realistic driving current than somatic current injection. Inhibition by the VML cell was simulated with 100 inhibitory $GABA_a$ synapses distributed in a graded manner along the apical dendritic tree such that <5% were proximal to the soma (Maler et al., 1981). We drove the cell with a range of excitatory synaptic input frequencies combined with dendritic inhibitory synapses firing at 100 or 200 Hz (the maximum firing frequency of VML cells *in vitro*) (our unpublished observation). This led to a division of the FI curve, which increased with the frequency of inhibitory stimulation (Fig. 5*A*,*B*). Note that these results mirror the divisive effects that were induced by a deterministic shift in dendritic leak conductance (Fig. 3*E*). We can therefore conclude that unbalanced random dendritic inhibition is capable of the same divisive computation seen in our previous experiments. Additionally, the division still functions in the more natural scenario in which the excitation is dendritic in origin, rather than injected somatically.

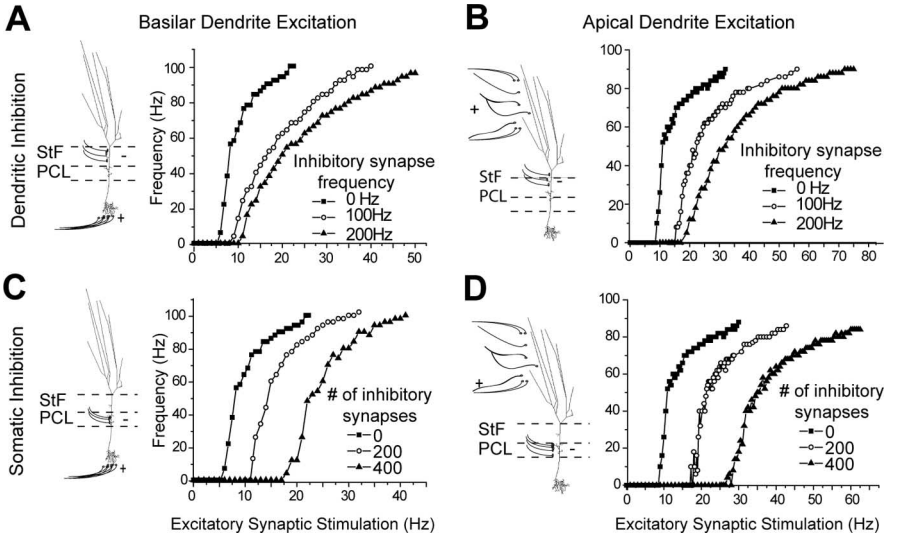

Figure 5. Stochastic inhibitory synaptic bombardment of the dendrite induces divisive gain control without balancing. ***A***, The model cell is driven by excitatory inputs to the distal basilar dendrite, combined with inhibitory synaptic inputs to the proximal apical dendrite. This combination leads to a divisive control of gain, in which gain decreases with increasing inhibitory frequency (100 Hz, ○; 200 Hz, ▲). Both conditions are divisively modulated relative to control (■). ***B***, When excitatory synaptic drive is moved to the apical dendrite, a subtractive effect occurs in combination with the divisive effects when paired with inhibitory conductances in the dendrite (100 Hz, ○; 200 Hz, ▲). Both conditions are divisively modulated relative to control (■). ***C***, ***D***, In comparison, placing the inhibitory synapses onto the soma [200 (○) and 400 (▲) synapses] leads to a subtractive rather than divisive shift relative to control (■) regardless of the site of excitation. Schematic diagram to the left of each frame indicates a basilar pyramidal cell in relation to the sites of synaptic inhibition or excitation. Dashed lines indicate the fiber bundles that define the regions of the pyramidal cell body (PCL) and the stratus tractum fibrosum (StF), which separates the proximal dendritic from the somatic region.

To simulate the greater number of sources of somatic inhibition existing in the ELL (Maler and Mugnaini, 1994), we attached more inhibitory synapses to the somatic compartment. Somatic inhibition, despite the slight increase in stochastic forcing resulting from the noisy inhibitory conductances being placed closer to the site of spike initiation, showed a subtractive computation with apical or basilar dendritic excitation (Fig. 5*C*,*D*) in this noisy regime. We note that this does not contradict previous studies of noise-induced gain control, which have either required a small number of synaptic inputs paired with somatic inhibition (Mitchell and Silver, 2003) or used a combination of dendritic excitation and somatic inhibition and a third current source (Prescott and De Koninck, 2003) to divisively modulate firing. The differences in the effects of stochastic somatic inhibition between these studies and our own are solely attributable to these differences in parameters.

These results demonstrate that in a realistic noisy regime for our system, our deterministic method of gain control has a greater effect than noise alone, because the highest noise condition showed the least gain change. Instead, even under synaptic stimulation conditions, dendritic regulation of the somatic AHP successfully controlled gain without the requirement for synaptic balancing. This provides a mechanism for the division of firing rate without the deleterious effects of noise.

Discussion

Modulation of gain is of great importance to computations performed by the nervous system (Reichardt, 1961; Salinas and Sejnowski, 2001). We have shown a deterministic gain control mechanism based on dendritic inhibition. Specifically, a multiplicative effect (e.g., feedback excitation resulting from the DAP) is scaled down by dendritic inhibition, leading to an ultimate divisive effect. Compartmental modeling and analytics show that this mechanism provides a graded control of the responsiveness of the cell and follows the rules expected for a mechanism of divisive gain. Although it has been shown that the AHP is capable of regulating default gain (Troyer and Miller, 1997; Smith et al., 2002), we show here that feedback from active dendritic conductances can scale the size of the AHP allowing for fast changes in the gain of the cell. Additionally, a spatial segregation of inhibitory inputs to distinct compartments allows for a separation of computations: somatic inhibition allows for algebraic subtraction, whereas dendritic inhibition allows for divisive control of gain.

Previous experiments and modeling studies have shown the ability to obtain divisive gain control through noisy synaptic input using balanced inputs or dendritic saturation to maintain a stationary rheobase (Chance et al., 2002; Prescott and De Koninck, 2003). However, even small differences in balancing can alter rheobase as well as gain (Shu et al., 2003). Alternatively, unbalanced excitatory inputs can be sufficient to offset a tonic inhibitory conductance, but this mechanism functions only with small numbers of excitatory inputs (Mitchell and Silver, 2003). Such balancing is not required in the mechanism described here. Balanced, noisy conductances changes can, and do, have divisive

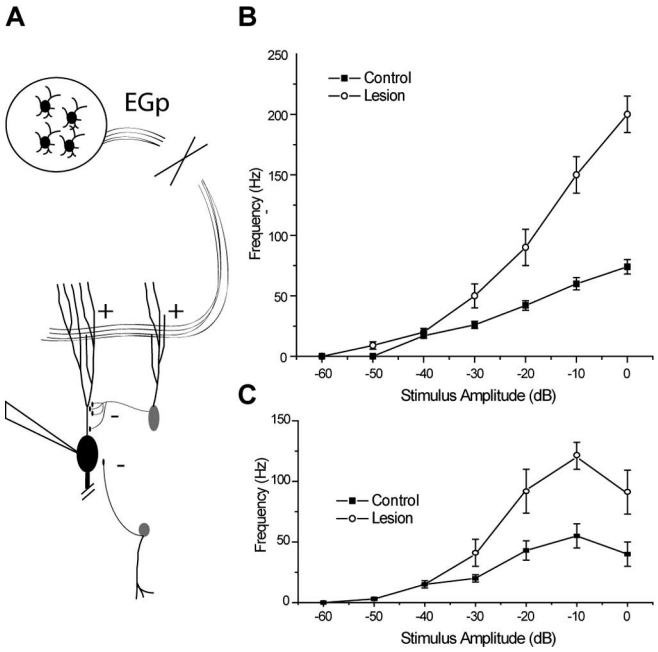

Figure 6. Divisive gain modulation *in vivo* involves the eminentia granularis pars posteriori (EGp) feedback pathway. ***A***, Diagram of the lesions performed by Bastian (1986). A lesion of the excitatory pathway projecting from EGp granule cells removes excitatory inputs to both the pyramidal and VML cells. ***B***, ***C***, Multiplicative gain changes after lesions described in ***A***. Pyramidal cells responding preferentially to either upstrokes (***B***) or downstrokes (***C***) in external electric fields communicated by peripheral electroreceptors are more strongly excited at high levels of stimulation after lesion, but firing rate is unchanged at low levels of stimulation. The suggested role of the VML cell in divisive gain control provides an explanation for the apparently paradoxical effects of this manipulation. Data are from the study by Bastian (1986).

effects on gain, but imperfections in balancing can have significant effects on rheobase. We show a mechanism that is minimally subtractive, because modulation of the gain occurs after spiking has already been initiated. Separation of the site of inhibition from the site of spike initiation also leaves the integrative properties of the somatic membrane unchanged, allowing gain to be modulated with minimal changes in either rheobase or filtering properties of the membrane.

A previous study of a neuron of the fly visual system showed divisive regulation of membrane voltage by dendritic inhibition in the nonspiking lobular plate tangential cells (Single et al., 1997), but this would not be expected to carry over to the spiking regime. A model developed to account for multiplicative computations in the locust included dendritic subtraction in the subthreshold domain; multiplication of inputs also required nonlinear transformations by spiking conductances (Gabbiani et al., 2002). This model represents an entirely different multiplicative function that does not require backpropagating spikes and DAPs or control of the gain of the firing mechanism.

Divisive gain control has been shown explicitly *in vivo* in the ELL (Bastian, 1986), and our results may explain some apparently paradoxical observations in this system. A lesion of a descending excitatory parallel fiber tract that terminates in the dendritic regions of the ELL (Fig. 6*A*) increased gain multiplicatively (Fig. 6*B*,*C*), despite the primarily excitatory nature of this parallel fiber tract *in vitro* (Berman and Maler, 1999; Lewis and Maler, 2002) and *in vivo* (Bastian, 1998). Previous work has shown this tract to have a significant role in stimulus cancellation on a time scale of seconds, which would not predict a divisive role (Bastian, 1996a,b, 1998; Bastian et al., 2004). Instead, we suggest that the parallel fibers also excite ELL interneurons that exclusively inhibit the proximal apical dendrites of pyramidal cells (Maler et al., 1981; Berman and Maler, 1999). The work presented here suggests that inhibition at this site will divide output firing rates. Thus, the removal of the excitatory drive to these cells by cerebellar lesions would be expected to eliminate the divisive gain that results from proximal dendritic inhibition and thus explain the multiplicative results observed after lesion (Bastian, 1986).

It has been suggested that tonic inhibition can have an inherent divisive effect caused by a nonlinear preprocessing of the input and a power-law voltage-firing rate relationship induced by background noise (Murphy and Miller, 2003). Because the divisive gain control effects were reproduced in slice experiments in which all preprocessing is absent, we can therefore discount this mechanism as contributing to the effects we observed.

Other models examining gain have included synaptically triggered forward-propagating dendritic spikes that are either inhibited (Archie and Mel, 2000) or recruited (Larkum et al., 2004). In the study by Archie and Mel (2000), synaptic input triggers forward propagating dendritic spikes and inhibition reduces the rate of these spikes rather than their amplitude, reducing excitatory drive to the cell. Evidence from *in vitro* studies of neocortical pyramidal cells has shown that the site of current injection along the apical dendrite can influence the gain of the firing through the all-or-none recruitment of dendritic spikes rate (Larkum et al., 2004) and subsequent bursts of activity. Because these dendritic spikes originate independently of the somatic spike, they cannot satisfy the mechanism we describe here. Notably, when noise is absent, the gain change is all-or-none and is associated with a large change in rheobase. A study of a pyramidal cell compartmental model demonstrated that combining saturating dendritic excitation with noisy somatic shunting inhibition can lead to gain control (Prescott and De Koninck, 2003). This form of divisive regulation is stochastic, in contrast to our deterministic method of DAP/AHP scaling. Therefore, the dendritic mechanisms described above either remain fundamentally stochastic or do not regulate the gain of the firing mechanism and are thus distinct from our hypothesized mechanism.

General applicability

There are three basic requirements for our proposed mechanism to work, and any cell with all three should be able to regulate gain via dendritic input. First, an active dendrite that can generate a backpropagating spike. Dendritic spikes appear to always be wider than somatic spikes, with their peaks occurring later (Reyes, 2001). This difference in membrane potential between the dendritic and somatic compartments obligatorily creates a brief positive dendrosomatic current, producing some DAP at the soma. Many cell types show strong DAPs (Nunez et al., 1993; Kang and Kayano, 1994), easily visible in the membrane voltage trace that have been shown or suggested to be a result of active dendritic conductances (Turner et al., 1994; Larkum et al., 1996; Magee and Carruth, 1999). Although a DAP might not be easily visible in the membrane voltage trace of many cells, active dendritic backpropagation should always provide some degree of dendrosomatic current flow. In many of our traces, the DAPs were not visible in the voltage trace until their contribution was revealed by blockade of active dendritic conductances. Thus, we do not expect that a cell has to exhibit a visually prominent DAP to display this kind of gain control, but some contribution of dendritic current from active dendrites is required.

A second requirement is some way of controlling the size of

the DAP. In our case, dendritic inhibition is capable of reducing the contribution of current to the soma. In both CA1 pyramidal cells and the mitral cell, dendritic inhibition can reduce the dendritic action potential (and therefore the reciprocal dendrosomatic current flow) (Tsubokawa and Ross, 1996; Lowe, 2002).

The third requirement for our proposed mechanism is that the response to a DAP is always to advance the timing of the next spike (e.g., a type I membrane) (Ermentrout, 1996). Interestingly, in some cells, an excitatory pulse immediately after spiking can delay the onset of the next spike (Hansel et al., 1993). Such a mechanism would invert the effects of the spike-triggered dendrosomatic current flow described here, leading to inherent divisive effects, the reduction of which by dendritic inhibition would cause a net multiplicative effect. The simplicity of this gain control mechanism is demonstrated by the reproduction of the key effect by an LIF model (Fig. 4). This guarantees that the mechanism does not depend on the complicated assortment of nonlinear ionic currents present in both real and the compartmental model of ELL pyramidal cells but can in fact be reduced to the above three rules. This reduction shows that the "divisive" computation performed by this mechanism is in fact a more complex operation rather than a simple scaling factor applied equally across the firing range of the cell.

Cortical cells in particular show the basic biophysical and anatomical requirements for displaying the deterministic gain control shown here. They have active dendritic sodium conductances (Stuart and Sakmann, 1994), and spike timing is advanced by excitation (Reyes and Fetz, 1993). Recent work has shown that balanced conductance fluctuations can attenuate backpropagating spikes in neocortical dendrites (Williams, 2004). Additionally, the neocortex includes inhibitory interneurons exclusively contacting the soma or the dendrites (Markram et al., 2004). Such spatial segregation of synaptic inputs may allow the same computations we observe to be performed in the cortex.

We suggest that because of the biophysical simplicity of the mechanism and the ubiquity of its elementary components, many cell types have the potential to display this type of dendritic scaling of a DAP, leading to a division of neuronal output.

References

Archie KA, Mel BW (2000) A model for intradendritic computation of binocular disparity. Nat Neurosci 3:54–63.

Baranauskas G, Tkatch T, Nagata K, Yeh JZ, Surmeier DJ (2003) Kv3.4 subunits enhance the repolarizing efficiency of Kv3.1 channels in fast-spiking neurons. Nat Neurosci 6:258–266.

Bastian J (1986) Gain control in the electrosensory system mediated by descending inputs to the electrosensory lateral line lobe. J Neurosci 6:553–562.

Bastian J (1996a) Plasticity in an electrosensory system. I. General features of a dynamic sensory filter. J Neurophysiol 76:2483–2496.

Bastian J (1996b) Plasticity in an electrosensory system. II. Postsynaptic events associated with a dynamic sensory filter. J Neurophysiol 76:2497–2507.

Bastian J (1998) Plasticity in an electrosensory system. III. Contrasting properties of spatially segregated dendritic inputs. J Neurophysiol 79:1839–1857.

Bastian J, Chacron MJ, Maler L (2004) Plastic and nonplastic pyramidal cells perform unique roles in a network capable of adaptive redundancy reduction. Neuron 41:767–779.

Berman NJ, Maler L (1999) Neural architecture of the electrosensory lateral line lobe: adaptations for coincidence detection, a sensory searchlight and frequency-dependent adaptive filtering. J Exp Biol 202:1243–1253.

Blomfield S (1974) Arithmetical operations performed by nerve cells. Brain Res 69:115–124.

Burkitt AN, Meffin H, Grayden DB (2003) Study of neuronal gain in a conductance-based leaky integrate-and-fire neuron model with balanced excitatory and inhibitory synaptic input. Biol Cybern 89:119–125.

Carandini M, Heeger DJ (1994) Summation and division by neurons in primate visual cortex. Science 264:1333–1336.

Chance FS, Abbott LF, Reyes AD (2002) Gain modulation from background synaptic input. Neuron 35:773–782.

Doiron B, Longtin A, Turner RW, Maler L (2001a) Model of gamma frequency burst discharge generated by conditional backpropagation. J Neurophysiol 86:1523–1545.

Doiron B, Longtin A, Berman N, Maler L (2001b) Subtractive and divisive inhibition: effect of voltage-dependent inhibitory conductances and noise. Neural Comput 13:227–248.

Ermentrout B (1996) Type I membranes, phase resetting curves, and synchrony. Neural Comput 8:979–1001.

Gabbiani F, Midtgaard J, Knopfel T (1994) Synaptic integration in a model of cerebellar granule cells. J Neurophysiol 72:999–1009.

Gabbiani F, Krapp HG, Koch C, Laurent G (2002) Multiplicative computation in a visual neuron sensitive to looming. Nature 420:320–324.

Hansel D, Mato G, Munsiel C (1993) Phase reduction in neural modelling. Concepts Neurosci 4:192–210.

Hines ML, Carnevale NT (1997) The NEURON simulation environment. Neural Comput 9:1179–1209.

Holt GR, Koch C (1997) Shunting inhibition does not have a divisive effect on firing rates. Neural Comput 9:1001–1013.

Kang Y, Kayano F (1994) Electrophysiological and morphological characteristics of layer VI pyramidal cells in the cat motor cortex. J Neurophysiol 72:578–591.

Koch C (1999) Biophysics of computation: information processing in single neurons. New York: Oxford UP.

Koch C, Poggio T (1992) Multiplying with synapses and neurons. In: Single neuron computation (McKeena T, Davis J, Zornetzer S, eds), pp 315–345. Orlando, FL: Academic.

Lapique L (1907) Recherches quantitatives sur l'excitation des nerfs traitee comme une polarization. J Physiol Pathol Gen 9:620–635.

Larkum ME, Rioult MG, Luscher HR (1996) Propagation of action potentials in the dendrites of neurons from rat spinal cord slice cultures. J Neurophysiol 75:154–170.

Larkum ME, Senn W, Luscher HR (2004) Top-down dendritic input increases the gain of layer 5 pyramidal neurons. Cereb Cortex 14:1059–1070.

Lemon N, Turner RW (2000) Conditional spike backpropagation generates burst discharge in a sensory neuron. J Neurophysiol 84:1519–1530.

Lewis JE, Maler L (2002) Dynamics of electrosensory feedback: short-term plasticity and inhibition in a parallel fiber pathway. J Neurophysiol 88:1695–1706.

Longtin A, Doiron B, Bulsara AR (2002) Noise-induced divisive gain control in neuron models. Biosystems 67:147–156.

Lowe G (2002) Inhibition of backpropagating action potentials in mitral cell secondary dendrites. J Neurophysiol 88:64–85.

Magee JC, Carruth M (1999) Dendritic voltage-gated ion channels regulate the action potential firing mode of hippocampal CA1 pyramidal neurons. J Neurophysiol 82:1895–1901.

Maler L (1979) The posterior lateral line lobe of certain gymnotoid fish: quantitative light microscopy. J Comp Neurol 183:323–363.

Maler L, Mugnaini E (1994) Correlating gamma-aminobutyric acidergic circuits and sensory function in the electrosensory lateral line lobe of a gymnotiform fish. J Comp Neurol 345:224–252.

Maler L, Sas EK, Rogers J (1981) The cytology of the posterior lateral line lobe of high-frequency weakly electric fish (*Gymnotidae*): dendritic differentiation and synaptic specificity in a simple cortex. J Comp Neurol 195:87–139.

Markram H, Toledo-Rodriguez M, Wang Y, Gupta A, Silberberg G, Wu C (2004) Interneurons of the neocortical inhibitory system. Nat Rev Neurosci 5:793–807.

Mitchell SJ, Silver RA (2003) Shunting inhibition modulates neuronal gain during synaptic excitation. Neuron 38:433–445.

Murphy BK, Miller KD (2003) Multiplicative gain changes are induced by excitation or inhibition alone. J Neurosci 23:10040–10051.

Nelson ME (1994) A mechanism for neuronal gain control by descending pathways. Neural Comput 6:242–254.

Nunez A, Florin A, Steriade M (1993) Electrophysiology of cat association

cortical cells in vivo: intrinsic properties and synaptic responses. J Neurophysiol 70:418–429.
Prescott SA, De Koninck Y (2003) Gain control of firing rate by shunting inhibition: roles of synaptic noise and dendritic saturation. Proc Natl Acad Sci USA 100:2076–2081.
Reichardt W (1961) Autocorrelation, a principle for the evaluation of sensory information by the central nervous system. In: Sensory communication (Rosenblith WA, ed), pp 303–317. Cambridge, MA: MIT.
Reyes A (2001) Influence of dendritic conductances on the input-output properties of neurons. Annu Rev Neurosci 24:653–675.
Reyes AD, Fetz EE (1993) Effects of transient depolarizing potentials on the firing rate of cat neocortical neurons. J Neurophysiol 69:1673–1683.
Salinas E, Sejnowski TJ (2000) Impact of correlated synaptic input on output firing rate and variability in simple neuronal models. J Neurosci 20:6193–6209.
Salinas E, Sejnowski TJ (2001) Gain modulation in the central nervous system: where behavior, neurophysiology, and computation meet. Neuroscientist 7:430–440.
Schwartz O, Simoncelli EP (2001) Natural signal statistics and sensory gain control. Nat Neurosci 4:819–825.
Shu Y, Hasenstaub A, Badoual M, Bal T, McCormick DA (2003) Barrages of synaptic activity control the gain and sensitivity of cortical neurons. J Neurosci 23:10388–10401.
Single S, Haag J, Borst A (1997) Dendritic computation of direction selectivity and gain control in visual interneurons. J Neurosci 17:6023–6030.
Smith MR, Nelson AB, Du Lac S (2002) Regulation of firing response gain by calcium-dependent mechanisms in vestibular nucleus neurons. J Neurophysiol 87:2031–2042.
Stuart GJ, Sakmann B (1994) Active propagation of somatic action potentials into neocortical pyramidal cell dendrites. Nature 367:69–72.
Tiesinga PH, Jose JV, Sejnowski TJ (2000) Comparison of current-driven and conductance-driven neocortical model neurons with Hodgkin-Huxley voltage-gated channels. Phys Rev E Stat Phys Plasmas Fluids Relat Interdiscip Topics 62:8413–8419.
Troyer TW, Miller KD (1997) Physiological gain leads to high ISI variability in a simple model of a cortical regular spiking cell. Neural Comput 9:971–983.
Tsubokawa H, Ross WN (1996) IPSPs modulate spike backpropagation and associated $[Ca^{2+}]i$ changes in the dendrites of hippocampal CA1 pyramidal neurons. J Neurophysiol 76:2896–2906.
Turner RW, Maler L, Deerinck T, Levinson SR, Ellisman MH (1994) TTX-sensitive dendritic sodium channels underlie oscillatory discharge in a vertebrate sensory neuron. J Neurosci 14:6453–6471.
Williams SR (2004) Spatial compartmentalization and functional impact of conductance in pyramidal neurons. Nat Neurosci 7:961–967.